

A length scale for non-local multi-scale gradient interactions in isotropic turbulence

Miguel P. Encinar[†]

Department of Mechanical Engineering, Johns Hopkins University, Baltimore, MD 21218, USA

(Received 21 May 2023; revised 14 August 2023; accepted 15 August 2023)

Three-dimensional turbulent flows enhance velocity gradients via strong nonlinear interactions of the rate-of-strain tensor with the vorticity vector, and with itself. For statistically homogeneous flows, their total contributions to gradient production are related to each other by conservation of mass, and so are the total enstrophy and total dissipation. However, locally, they do not obey this relation and have different (often extreme) values, and for this reason both production mechanisms have been subject to numerous studies, often decomposed into multi-scale interactions. In general lines, their dynamics and contributions to the cascade processes and turbulent kinetic dissipation are different, which poses a difficulty for turbulence modelling. In this paper, we explore the consequence of the ‘Betchov’ relations locally, and show that they implicitly define a length scale. This length scale is found to be approximately three times the size of the turbulent structures and their interactions. It is also found that, while the non-locality of the dissipation and enstrophy at a given scale comes mostly from larger scales that do not cancel, the non-local production of strain and vorticity comes from multi-scale interactions. An important consequence of this work is that isotropic cascade models need not distinguish between vortex stretching and strain self-amplification, but can instead consider both entities as part of a more complex transfer mechanism, provided that their detailed point value is not required and a local average of reasonable size is sufficient.

Key words: isotropic turbulence, turbulence theory, turbulence modelling

1. Introduction

Non-locality is an essential feature of turbulent flows. The term ‘non-local’ or ‘non-local interactions’ is used in turbulence research to refer to two distinct phenomena, non-local interactions in physical space, and in Fourier space. This paper focuses on the former.

[†] Email address for correspondence: miguel.pencinar@jhu.edu

The ultimate source of non-locality is the incompressibility assumption, which forces the velocity field to be solenoidal at each instant of time and point of space. Incompressibility acts through the pressure gradient term in the Navier–Stokes equation and thus it can be said that the pressure is responsible for non-locality. The only way for the velocity field to be able to satisfy the incompressibility condition is to communicate the movement of each fluid particle to all other particles instantly through the pressure. For this reason it seems that the most straightforward way of studying non-locality is studying the characteristics of the pressure field. Indeed, some works explore the characteristics of the isotropic pressure field directly (Batchelor 1953; Pumir 1994; Tsuji & Ishihara 2003), although often they are not concerned about non-locality in particular, although exceptions do exist (Wilczek & Meneveau 2014; Vlaykov & Wilczek 2019). Non-locality is instead typically studied in the context of enstrophy and dissipation amplification. These quantities evolve through strain–vorticity interactions, which are non-local, and through the pressure Hessian in the rate-of-strain evolution equation, which is also non-local. Both terms have been extensively studied, particularly in the context of non-locality (Ohkitani & Kishiba 1995; Tsinober 2000; Meneveau 2011; Wilczek & Meneveau 2014; Elsinga *et al.* 2017). Moreover, the equations of the filtered velocity gradients can be used to model inter-scale interactions, and non-locality here plays an important role, as inter-scale vortex stretching (VS) is often regarded as an important cascade indicator (Eyink 2005). There are also indications that strain-self amplification (SSA) is equally (or up to three times more) important for the cascade rate (Tsinober 2000; Carbone & Bragg 2020; Johnson 2020; Yang *et al.* 2023) than VS.

Both VS and SSA are known to balance on average (Betchov 1956), but locally can be very different from each other (Jiménez *et al.* 1993; Tsinober 2000). The same can be said for the enstrophy and the non-dimensional dissipation, whose total magnitudes are related to each other. In principle, this allows one to study dissipation using the field of enstrophy as a proxy and, traditionally, research has favoured the study of the ‘simpler’ vorticity vector over the more tedious rate-of-strain tensor.

The derivation of the evolution equations of the velocity gradients can, at most, hide the effect of the pressure term in other kinds of non-local interactions, e.g. VS, but cannot remove its impact. A particularly interesting attempt to separate local from non-local VS is Hamlington, Schumacher & Dahm (2008). This work exploits the integral transform from the vorticity to strain to produce local and non-local fractions of the VS. The same decomposition has been used by Buaria & Pumir (2021) to analyse very high-Reynolds-number turbulence, reaching the conclusion that most amplification comes from non-local interactions. These works have in common that a length scale needs to be chosen to separate local from non-local effects. Pressure is global in incompressible flows, making this length scale nominally infinite. Thus, the concept of defining a length scale associated with non-locality is ill posed. However, even if the effects of pressure need to be global, the magnitude of those effects across distance decays significantly, due to the properties of the Laplacian operator which appears in the equation for the pressure. This magnitude is important because non-locality hinders our ability to understand gradient amplification and to produce sensible cascade models. This length scale is studied in Vlaykov & Wilczek (2019), where the authors study the source term of the pressure fluctuations. Using correlations, they reach the conclusion that most of the non-locality arising from this term vanishes at distances larger than 20 Kolmogorov units.

In the present paper, we take a similar approach to them, seeking to create a sensible definition of non-locality in terms of velocity gradient interactions, and to measure the scale(s) at which non-locality is most intense, and more importantly, its scaling with the Reynolds number. Although ‘globality’ is required to fully satisfy the continuity




Name	N	$k\eta_{max}$	L_E/η	L_E/λ	$\epsilon L_E/u'^3$	Re_λ	N_{stat}	Symbol
S256	256	1.5	119	5.03	0.524	144	640	
S512	512	1.5	213	7.12	0.462	231	160	
S1024	1024	2.0	333	9.80	0.494	298	40	

Table 1. Detail of the numerical simulations used in the paper. Here, N is the number of grid points in each of the periodic directions, η is the Kolmogorov scale, L_E the integral scale, λ the Taylor microscale, ϵ is the total dissipation. All these quantities are computed as in Batchelor (1953). Further, N_{stat} refers to the number of approximately independent snapshots used to compute the statistics in this paper.

equation, we argue that the main dynamical effects of continuity in the velocity gradients have a marked length scale, and that said length scale is important for modelling the flow dynamics. The main objective is to provide a sensible measure of the distances in which non-local interactions are dominant, and when they may be neglected. We extend this analysis to the filtered velocity-gradient tensor, which allows us to generalise our conclusions from the dissipative range to the inertial one.

The remainder of the paper is structured as follows. Section 2 introduces the databases used for this paper, and § 3 recalls the equations that contain the quantities studied in this paper and their relation to Navier–Stokes. They are followed by § 4, which shows all the results regarding gradient non-locality. Finally, § 5 closes with the final discussion and conclusions of the manuscript.

2. Numerical databases

We use databases of homogeneous isotropic turbulence (HIT) obtained from direct numerical simulation of the incompressible Navier–Stokes equations. Simulations use a standard fully dealiased spectral spatial discretisation coupled with a third-order semi-implicit Runge–Kutta time stepper. Turbulence is forced with constant energy input at the largest wavenumber corona, $|\mathbf{k}| < 2$, where $|\mathbf{k}|$ is the wavenumber magnitude. Table 1 gathers the main characteristics of the simulations. The two lower Reynolds number (Re) simulations use a smaller resolution, $k\eta_{max} = 1.5$ than the *de facto* standard of two. Although simulations as low as $k\eta_{max} = 1$ have been used to gather useful statistics (Kaneda & Ishihara 2006, among others), high-order moments, such as the statistics of the third invariant, could be affected by this resolution. However, the good collapse of their statistics with the highest Re simulation, which is computed at the standard resolution, gives us confidence in the results of this paper. More details about the numerical method and simulations are provided in Cardesa, Vela-Martín & Jiménez (2017).

3. Gradient amplification and non-locality

Consider the incompressible Navier–Stokes equations

$$\partial_i u_i = 0, \tag{3.1}$$

$$D_t u_i \equiv \partial_t u_i + u_j \partial_j u_i = -\partial_i p + \nu \partial_{kk} u_i, \tag{3.2}$$

where u_i is the velocity vector, p the kinematic pressure and ν the kinematic viscosity; D_t stands for the material derivative. The kinematic pressure acts in (3.2) as a Lagrange multiplier, responsible for enforcing (3.1) at each time and point in space. The only source

of divergence in (3.2) is the term $u_j \partial_j u_i$, which is the divergence of the Reynolds-stress tensor, $\partial_j(u_i u_j)$. A possible interpretation is that the Reynolds stresses generate divergence, which is opposed and cancelled by the gradient of the pressure. However, this can be misleading, as both terms can be grouped together in the equation, and the nonlinear term of the Navier–Stokes equation is $\partial_j(u_i u_j + \delta_{ij} p)$, where δ is the Kronecker delta tensor. In this form, it can be seen explicitly that non-locality is a consequence of nonlinearity. Taking the gradient of (3.2) yields

$$D_t A_{ij} = -\partial_{ij} p - A_{ik} A_{kj} + \nu \partial_{kk} A_{ij}, \tag{3.3}$$

where $A_{ij} = \partial_j u_i$ is the velocity-gradient tensor. The latter can be further decomposed into a symmetric and skew-symmetric part, $A_{ij} = S_{ij} + \Omega_{ij}$, where the symmetric S_{ij} is the rate-of-strain tensor, and the skew-symmetric Ω_{ij} is the rate-of-rotation tensor. The latter is related to the vorticity vector by $\omega_i = -1/2 \varepsilon_{ijk} \Omega_{jk}$, where ω is the vorticity vector and ε is the totally skew-symmetric tensor. Evolution equations for S and ω can be constructed from (3.3)

$$D_t S_{ij} = -\partial_{ij} p + S_{ik} S_{kj} - \frac{1}{4}(\omega_i \omega_j - \omega^2 \delta_{ij}) + \nu \partial_{kk} S_{ij}, \tag{3.4}$$

$$D_t \omega_i = \omega_j S_{ij} + \nu \partial_{kk} \omega_i, \tag{3.5}$$

where $\omega^2 = \omega_i \omega_i$. Non-locality appears in (3.4) through the pressure Hessian, and in (3.5) through the VS term. The pressure is hidden in the vorticity equation through the strain–vorticity interactions, as strain and vorticity are related to each other by a non-local integral transform (Ohkitani 1994). Note that both equations are non-local in the convective term too, as obtaining the velocity field from either the vorticity or the rate of strain involves using the incompressibility condition and inverting a second derivative. The trace of (3.4) gives a recipe to compute the pressure

$$\partial_{ii} p = \frac{1}{2} \omega^2 - \mathbf{S}^2, \tag{3.6}$$

where $\mathbf{S}^2 = S_{ij} S_{ij}$. The pressure source term is proportional to the local imbalance of enstrophy and dissipation and, because for an isotropic flow the average pressure vanishes,

$$\frac{1}{2} \langle \omega^2 \rangle = \langle \mathbf{S}^2 \rangle, \tag{3.7}$$

where the brackets are the spatial average. Note that, for an isotropic flow with periodic or infinite boundaries, the spatial average is sufficient to satisfy (3.7). Equation (3.7) is an important non-local relation between the global enstrophy and the total dissipation. Equations for these two magnitudes can be obtained by contracting (3.4) and (3.5) with S and ω respectively and taking the average

$$\partial_t \langle \mathbf{S}^2 \rangle = -\langle S_{ij} S_{jk} S_{ki} \rangle - \frac{1}{4} \langle \omega_i S_{ij} \omega_j \rangle - \nu \langle S_{ij} \partial_{kk} S_{ij} \rangle, \tag{3.8}$$

$$\partial_t \langle \omega^2 \rangle = \langle \omega_i S_{ij} \omega_j \rangle - \nu \langle \omega_i \partial_{kk} \omega_i \rangle. \tag{3.9}$$

Production of enstrophy is achieved through the VS acting on the vorticity $\omega_i S_{ij} \omega_j$, which has to be positive on average in order to sustain turbulence. This term is a sink for the rate-of-strain magnitude, which in turn is produced by the term $S_{ij} S_{jk} S_{ki}$ or SSA, which has to be negative on average. The expectancies of both quantities are linked by the celebrated ‘Betchov’ relation (Betchov 1956)

$$\langle S_{ij} S_{jk} S_{ki} \rangle = \frac{3}{4} \langle \omega_i S_{ij} \omega_j \rangle. \tag{3.10}$$

This relation is purely kinematical, as only incompressibility, isotropy and the chain rule are required to prove it. As stated in the introduction, interpretations of (3.10) are

sometimes controversial. While some authors (e.g. Ohkitani 1994; Eyink 2005) effectively use to recast the production of (filtered) gradients solely in terms of VS, others (e.g. Tsinober 2001; Carbone & Bragg 2020; Johnson 2020) question its local implications, as SSA and VS play, in principle, different roles in the turbulence dynamics.

Equations (3.7) and (3.10) are the two most important kinematic relations which tie gradients and gradient production, respectively, across the flow field. Moreover, they have been recently shown to be the only two homogeneous kinematic constraints (Carbone & Wilczek 2022). They can be reworked exactly in terms of the average of the second and third invariants of the velocity gradient tensor, Q and R (Chong, Perry & Cantwell 1990)

$$\langle Q \rangle = -\frac{1}{2} \langle A_{ij} A_{ji} \rangle = \frac{1}{4} \langle \omega_i \omega_i - 2 S_{ij} S_{ij} \rangle = 0, \quad (3.11)$$

$$\langle R \rangle = -\frac{1}{3} \langle A_{ij} A_{jk} A_{ki} \rangle = -\frac{1}{3} \langle S_{ij} S_{jk} S_{ki} + \frac{3}{4} \omega_i S_{ij} \omega_j \rangle = 0. \quad (3.12)$$

Aside from the pressure Hessian, non-local kinematic constraints force the two invariants of the velocity gradient tensor to vanish. The first, which is the divergence of the velocity, is zero at each point in space due to incompressibility, and the spatial averages of the second or third are zero for an isotropic flow. In the following section, we explore how cancellation of Q and R occurs in isotropic flows, but first we recall the typical way in which non-locality manifests in the velocity gradients.

3.1. Evidence of non-locality

Figure 1(a) shows a three-dimensional picture portraying non-locality in terms of the velocity gradients. It contains a small subvolume of isotropic turbulence, with contours for enstrophy and dissipation. The picture suggests that they are spatially related to each other, but it can be seen that they are not collocated. These visual inspections are quantified by the joint probability density function (p.d.f.) of the enstrophy magnitude $|\omega|$ and the dissipation magnitude $2|S|$, both normalised by the root mean square of the vorticity $(\omega')^{1/2}$. They are shown in black contours in figure 1(b). Lighter grey contours contain the p.d.f. of both quantities if they were completely uncorrelated, obtained as the product of their probabilities, $P(\omega)P(S)$. Visually, it reveals that a correlation of $C(\omega, S) \approx 0.57$ between the two fields exists. It also shows that strong events happen in different places, giving the p.d.f. its characteristic ‘square’ shape. It has been known for some time that this is caused by strong vortices or ‘worms’ surrounded by the strong rate of strain induced by them, and is often as an archetypical example of gradient non-locality (Jiménez *et al.* 1993). Because vortices have a transverse length scale $O(\eta)$, the strain they induce must have the same length scale (Burgers 1948). Thus, it is reasonable to expect that both quantities should correlate at lengths of the same order. Blue contours show the joint p.d.f. of $\langle |\omega|^2 \rangle_{12\eta}^{1/2}$ and $\langle 4|S|^2 \rangle_{12\eta}^{1/2}$. These quantities are the averaged squared norm of enstrophy and dissipation in spherical subvolumes of radius 12η . Both quantities correlate much better, with a correlation of $C \approx 0.86$. Finally, the orange contours show that this property not only applies to events of average intensity but also to extreme ones. They represent the joint p.d.f. of the maximum value of the variables within the same spheres of radius 12η , and the correlation is similar to the one for the averages. These values are computed by taking the maximum value of each quantity instead of taking the average value within the ball. As noted in Buaria & Pumir (2022), there is a non-unity power law relating the intensity of $|\omega|$ and $|S|$, which can be shown here as a different covariance between the blue and the orange contours.

Figure 1(c) extends this analysis to the joint p.d.f. of VS and SSA, with its characteristic star shape. Most of the conclusions from figure 1(b) carry over here. Both VS and SSA can

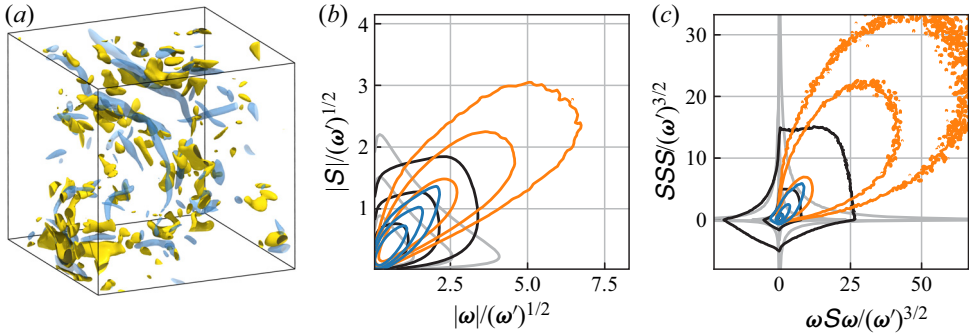


Figure 1. (a) Subvolume of $(250\eta)^3$ of a snapshot of S256 (see table 1). Blue isosurfaces are $|\omega| > 4(\omega')^{1/2}$ and yellow ones $|S| > 4(\omega')^{1/2}$. (b) Joint p.d.f.s of the enstrophy magnitude $|\omega|$ and the dissipation magnitude $|S|$. (c) Joint p.d.f.s of the VS and the SSA. (b,c) Contours contain 90, 99 and 99.9 % of the probability mass. Black contours are the regular joint p.d.f. and grey contours are the product of the probabilities of the individual p.d.f. of the magnitudes. Ball coarse-grained quantities in a 12η radius are shown in blue and orange contours, the average is taken for the blue ones and the maximum is taken for the orange ones. In panels (a–c) ω' stands for the variance of the vorticity.

change sign and thus local averages can too. However, the probability of finding gradients being depleted diminishes significantly when the average is taken over volumes of 12η , from 57 % and 50 % of the S512 domain having negative VS and positive SSA respectively, to 1.5 % and 1 % when $\langle \omega S \omega \rangle_{12\eta}$ and $\langle SSS \rangle_{12\eta}$ are considered. Correlations between the two variables improve by almost the same margins as $\langle |\omega|^2 \rangle_{12\eta}^{1/2}$ and $\langle 4|S|^2 \rangle_{12\eta}^{1/2}$.

While figure 1 shows that non-locality has a strong mark in turbulent velocity gradients, it also suggests that a sensible portion of the non-local ‘Betchov’ relations cancel over small distances within the dissipative range. Thus, cancellation implicitly defines a distance relating the components of the invariants, which we explore in § 4.

4. Cancellation of the velocity-gradient invariants

Figure 2(a) shows $\langle Q \rangle'_r$ for the three available Reynolds numbers, which stands for the variance (\prime) of the coarse-grained Q , defined as

$$\langle Q \rangle'_r = \frac{1}{V} \int_V \langle Q \rangle_r^2 dx_i, \tag{4.1}$$

where V stands for the computational domain. Note that the mean needs not to be subtracted because $\langle Q \rangle_r$ vanishes when integrated over the volume. The coarse grain follows Eyink (2005), averaging Q over a sphere of radius r . When the radius goes to zero, we recover Q' , and when $r \rightarrow \infty$, $\langle Q \rangle'_\infty$ must vanish due to incompressibility. Thus, $\langle Q \rangle'_r$ is a measure of how far the local enstrophy-dissipation balance is from the global one. Our results are very similar to the findings of Vlaykov & Wilczek (2019), showing that most of the cancellation occurs within spheres of $r \approx 20\eta$, which encompass a vortex core and the strain it induces. The inset corresponds to the same curves, but in log–log scale. They are normalised with the surrogate dissipation $D = (u')^{3/2}/L_E$, which makes their tails collapse. The curves shown stop at $r/L_E \approx 1.6$ because we want to avoid the forced integral scale. The black line is a fitted power law that corresponds to $p \approx r^{-3.02 \pm 0.1}$, and approximately holds for the three Reynolds numbers. The tails should be compared with the dashed red line, obtained from randomising the relative positions of the dissipation and

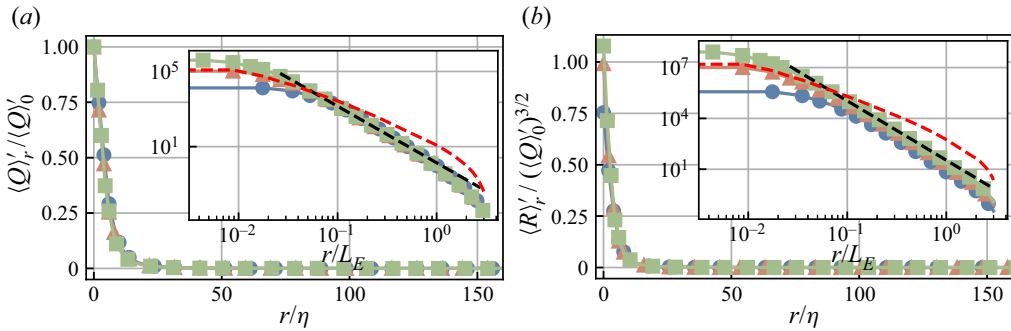


Figure 2. Variance of (a) $\langle Q \rangle_r$ and (b) $\langle R \rangle_r$ as a function of the integration radius for the three Reynolds numbers. The insets are log–log plots of the same data, but normalised with the integral time scale in the abscissa, and using the surrogate dissipation instead of $\langle Q \rangle_0$ in the ordinate. The red dashed line corresponds to the randomised test of S512.

entropy before computing Q . This artificial field of Q still satisfies Betchov’s equality, but assumes no spatial relation between its two components. Its power law is $p \approx r^{-2.0}$, which corresponds to the growth of the surface of the integration sphere, and thus it cancels over larger length scales. Figure 2(b) is equivalent to 2(a) but shows $\langle R \rangle_r$. It is normalised with $\langle Q \rangle_0^{3/2}$, which results in intermittency effects showing at $r \rightarrow 0$, even at our moderate Reynolds numbers. These effects cancel quickly with the coarse graining, and R roughly satisfies Betchov’s equality for the same radius of Q . However, the fitted power law is slightly different $p \approx r^{-3.5 \pm 0.15}$, which results in a faster cancellation. This figure shows that strong VS events are always accompanied by strong SSA events in their neighbourhood, and that the typical length scale of this interaction is of the same order as the interactions of the dissipation and strain objects.

4.1. Multi-scale analysis of the Betchov invariants

The results so far agree with those of Vlaykov & Wilczek (2019) and extend theirs to R , with similar conclusions. The cancellation of Q is a consequence of vorticity generating strain or *vice versa*, and can be interpreted as both entities being part of the same structure, i.e. a strong vortex with its self-induced strain (Elsinga & Marusic 2010). In the same way, the fact that the same cancellation holds for the VS and the SSA implies that the latter are paired somewhat locally, and that they probably come from the same dynamics, which generates them at the same time. In order for this to hold for the turbulent cascade, the same balance should hold at all inertial scales.

This is explored in figure 3, which shows spherical averages similar to figure 2, but for the invariants of the filtered velocity fields. First, the velocity fields are filtered using a family of isotropic Gaussian kernels, with their widths separated in powers of two, and ranging from 10η to the integral scale

$$\tilde{u}_i(x_j) = \frac{1}{(\Delta\sqrt{\pi})^3} \int_V \exp[-((x_j - \xi_j)/\Delta)^2] u_i(\xi_j) d\xi_j, \quad (4.2)$$

where Δ serves as the filter width. The invariants of the filter velocity, \tilde{Q} and \tilde{R} represent the same incompressibility balances (and topology), but for the filtered velocity (Eyink 2005; Leung, Swaminathan & Davidson 2012; Lozano-Durán, Holzner & Jiménez 2016; Danish & Meneveau 2018). We repeat the coarse graining of integrating both quantities in growing spheres of radius r , until we reach the integral scale. Although the fact that

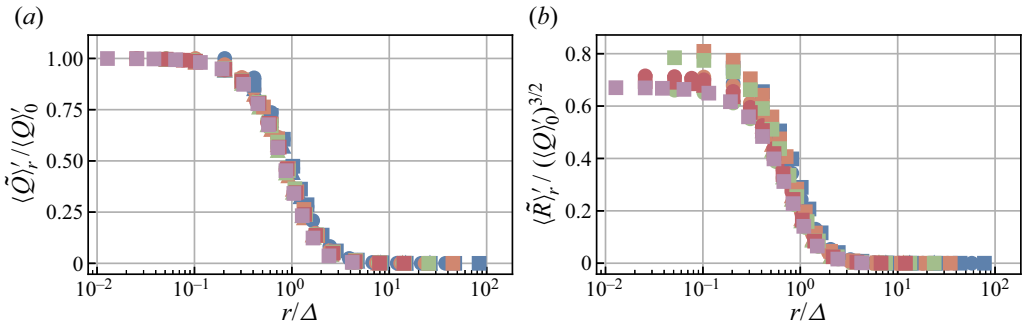


Figure 3. Variance of (a) $\langle \tilde{Q} \rangle_r$ and (b) $\langle \tilde{R} \rangle_r$ as a function of the integration radius for the three Reynolds numbers and various filters. See § 4.1 for more details.

we are coarse graining the fields twice may be striking, it should be clarified that both operations have different purposes. Filtering the velocity is an attempt to study the gradient interactions at the scale of the filter, which are otherwise hidden by the smaller scale gradients. Coarse graining the invariants (which are nonlinear functions of the velocity field) pursues the study of how local the balance between the components that form the invariants is. Figure 3(a) shows $\langle \tilde{Q} \rangle_r$ for every filter width that satisfies $30\eta < \Delta < 0.5L_E$, and it is considered to fall within the inertial range. These are five, six and seven filters for S256, S512 and S1024, respectively. They are normalised with \tilde{Q}' . When the radius r is normalised with Δ , all the curves collapse very well. At $r/\Delta \approx 3$, more than 95 % of the cancellation has taken place. Similar numbers are given by figure 3(b), which shows $\langle \tilde{R} \rangle_r$. Again, it shows intermittency effects, with the ratio of \tilde{R}' over $(\tilde{Q}')^{3/2}$ being larger the farther the filter width is from the integral scale. Despite these effects, most of the cancellation still happens at distances smaller than three filter widths.

The fact that the cancellation or ‘Betchov’ length scale is the same for both invariants may mislead the reader to think that they occur within the same spheres, i.e. that they are part of the same ‘structure’. However, we found that the cancellation of $\langle Q \rangle$ and $\langle R \rangle$ is not collocated, meaning that the fact that enstrophy and dissipation are in local equilibrium does not imply that VS and SSA are, and *vice versa*. Figure 4 explores their relation by showing the p.d.f. of the minimum distance across local minima of $\langle Q \rangle_{r/\eta=20}$ and $\langle R \rangle_{r/\eta=20}$. They are computed as follows. First, the local minima are identified by looking for zeros of the gradient of the $\langle Q \rangle_{r/\eta=20}^2$ and $\langle R \rangle_{r/\eta=20}^2$ fields (note that the means of these fields are the variances as defined in (4.1)). Then, for each of the two fields, we retain the minima which are closest to zero in magnitude (closer to local equilibrium), until the density of retained minima in the field is a constant. The latter is such that the average distance between minima, or to the minima of the other quantity, is 20η , which is the radius of the coarse graining. Changing this density to twice or half its value does not change the results, as long as they are renormalised with the new density. These sets of points represent the centres of regions where either Q or R are in local equilibrium. The minimum distance between these minima gives us information about the organisation of the regions where the Betchov relation is satisfied locally for each quantity. The random Poisson model for the distance between randomised points is shown as a dashed line, which would match the data if no relation existed between the set of local minima of $\langle Q \rangle_{r/\eta=20}$ and the local minima of $\langle R \rangle_{r/\eta=20}$. The data, however, do not fit a Poisson process, and instead show a much larger tail to the right, falling from a flat plateau in the range of one

A length scale for non-local gradient interactions in HIT

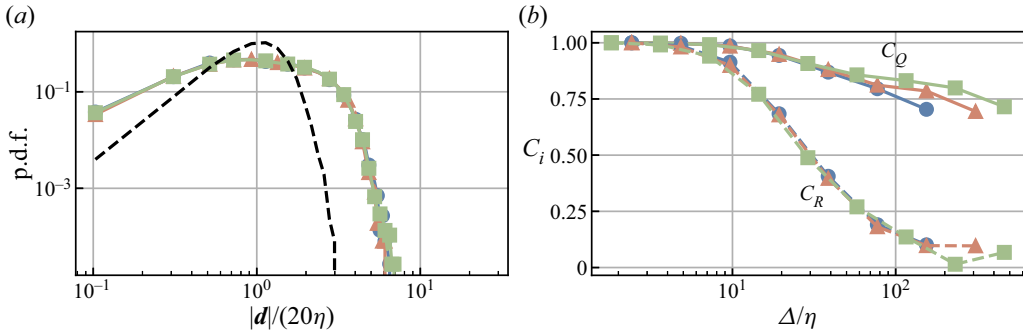


Figure 4. (a) The p.d.f. of the distance between the minima of $\langle Q \rangle|_{\Delta/\eta=30}$ and $\langle R \rangle|_{\Delta/\eta=30}$. (b) Correlations between the filtered and coarse-grained velocity-gradient invariants. Lines with circles are for the second invariant and dashed lines with squares are for the third.

to three times the coarse-graining length. The expectancy of the distance is $1.63r$, and it is consistent for the three Reynolds numbers. This organisation shows that the equilibria of both quantities are related to each other, and that they tend to be further apart than a random process. Although physically unsound, the reader may find it useful to think of both sets of points as if they were repelling or avoiding each other. If we interpret the flow in terms of the evolution equations for the gradients, then dissipation and enstrophy represent structures or eddies, and VS and SSA their interactions. The fact that they are not collocated highlights that interactions of multiple ‘ Q ’ objects are required to produce ‘ R ’ ones.

Consider now figure 4(a). It shows the correlation between the filtered invariants and the coarse-grained ones

$$C_Q(\Delta) = \frac{\int_V \tilde{Q}(x_i) \langle Q \rangle_{\Delta}(x_i) dx_i}{\left(\int_V \langle Q \rangle_{\Delta}(x_i) \langle Q \rangle_{\Delta}(x_i) dx_i \int_V \tilde{Q}(x_i) \tilde{Q}(x_i) dx_i \right)^{1/2}}, \quad (4.3)$$

and equivalently for R . The filter width of the Gaussian is chosen to match Δ , so both quantities have comparable scales. These two quantities, \tilde{Q} and $\langle Q \rangle_{\Delta}$, although they may seem similar, have very different meanings. While $\tilde{Q}(x_i; \Delta)$ represents the local balance of dissipation and enstrophy for scales larger than Δ at the position x_i , $\langle Q \rangle_{\Delta}(x_i; \Delta)$ represents the excess of Q needed to be cancelled in order to satisfy the kinematic relation locally, after scales below Δ have been cancelled. This is not an effect of the difference between the coarse graining and the filtering kernel, but one that comes from the step at which this operation is performed. While $\langle Q \rangle_{\Delta}(x_i; \Delta) = -1/2 \langle A_{ij} A_{ji} \rangle_{\Delta}$ is constructed from the total velocity field, $\tilde{Q} = -1/2 \tilde{A}_{ij} \tilde{A}_{ji}$ comes from the contraction of the filtered velocity gradient tensor. The correlations are shown to collapse as a function of Δ/η , except for the scales $\Delta/L_E \sim 1$, which do so when normalised with the integral scale. These large scales show approximately a constant correlation coefficient for all three Reynolds numbers that is approximately equal to 0.75. For Q , the correlation is approximately unity for scales smaller than 10η , and decays smoothly into the large scales. The fact that this correlation coefficient is large implies that most of the structure of $\langle Q \rangle$ comes from \tilde{Q} . This can be interpreted as the enstrophy-dissipation balance at scales larger than the filter being most responsible for the lack of local kinematic balance. It suggests a picture, when paired with

figure 3(a), in which, at each scale, local balance is approximately satisfied within a few filter widths, and the excess comes from the scales above the filter.

A similar analysis can be done for \tilde{R} and $\langle R \rangle$, and it is shown using dashed lines. The correlation decays far from the dissipative range, and the fields of both quantities are essentially uncorrelated at the integral scale. This result shows that the self-scale interactions at larger scales cannot be the main contribution to the balance of gradient amplification and that multi-scale contributions, i.e. amplification of gradients at one scale due to the gradients at a different one, are the most important contribution, in agreement with Buaria & Pumir (2021). Multi-scale interactions are part of the turbulent cascade, which can be expressed in terms of the filtered gradient production terms (Johnson 2020). Although evaluating those terms is out of the scope of the present paper, they can be compared with the excess of Betchov's balance using the multi-scale procedure of Yang *et al.* (2023), for example.

5. Discussion and conclusions

We have shown that most of the kinematic balance between the enstrophy and the dissipation, and between the VS and the SSA, is satisfied within spheres of radius of the order of 20η . For their counterparts computed from the filter velocities, cancellation is achieved at lengths of the order of three filter widths, for as long as the filter width lies within the inertial range. The remaining imbalance correlates well with the filtered source in the case of the second invariant but notably worse for the third.

If the filter width is considered representative of the size of the structures captured by the filter, then the 'Betchov' length scale is approximately three times the size of an 'eddy', both for the second and the third invariants. The former can be interpreted as representative of turbulent structures comprised vorticity surrounded by strain, balancing in three times the typical width of either the vorticity or the strain structures. The latter represents the interaction of vorticity and strain structures, resulting in the production of both VS and SSA, which also balance within three times their size. The same arguments hold for the unfiltered invariants, as $7-10\eta$ is the typical size of vortices and strain sheets.

The conclusion is that, for isotropic flows, or isotropic cascade models, the assumption that dissipation can be replaced by enstrophy, or SSA by VS (e.g. Eyink 2005), is physically reasonable, even if dynamically they are completely different quantities. This statement only holds if the point value of the components is not considered dynamically relevant and only its effect in a small neighbourhood is considered. The present results suggest that VS and SSA should be modelled or studied as part of a larger dynamical mechanism 'the vortex-strain amplification' which, while necessarily not local, is approximately balanced in a small neighbourhood of a reasonable size $r/\Delta \approx 3$.

This idea is also supported by the fact that their proportion can be attributed solely to kinematic relations (Yang *et al.* 2023). A sensible model compatible with the successful ideas of the multiplicative cascades is that enstrophy-dissipation objects, i.e. vortices and their induced strain, interact with each other; generating VS-SSA mechanisms at various scales. This is supported by two findings. First, the fact that the local balance of Q is not collocated with the local balance of R , and that their distributions are not independent of each other. It is also compatible with the power laws of figure 2. Second, the present results suggest that most of the excess imbalance of enstrophy and dissipation comes from larger scales. However, that is not true for the VS-SSA pair, which implies that the imbalance must come from interscale interactions. Additional work should clarify whether, for

example, these interactions happen in a neighbourhood in scale space (Cardesa *et al.* 2017), or are fully global in this sense.

Finally, we would like to note that, while it is perfectly possible to measure the contributions of both VS and SSA to the turbulent cascade, it seems of less dynamic relevance than their combined contributions acting over a broader region in isotropic flows. This distinction, however, may be necessary to model non-isotropic flows under strong shear, where the balance may not be satisfied at the length scales shown here.

Acknowledgements. The author would like to thank Dr A. Vela-Martín and B. Jiménez-Carrasco for their useful comments in a preliminary version of this manuscript, and the three anonymous referees who helped polish this paper to its final version. I would also like to thank Professor J. Jiménez for providing the computational resources used for this work.

Funding. The author received no specific grant from any funding agency. The computational resources have been provided by the ERC.2020.AdG.101018287, ‘CausT’.

Declaration of interest. The authors report no conflict of interest.

Author ORCIDs.

 Miguel P. Encinar <https://orcid.org/0000-0002-3007-5981>.

REFERENCES

- BATCHELOR, G.K. 1953 *The Theory of Homogeneous Turbulence*. Cambridge University Press.
- BETCHOV, R. 1956 An inequality concerning the production of vorticity in isotropic turbulence. *J. Fluid Mech.* **1** (5), 497–504.
- BUARIA, D. & PUMIR, A. 2021 Nonlocal amplification of intense vorticity in turbulent flows. *Phys. Rev. Res.* **3** (4), L042020.
- BUARIA, D. & PUMIR, A. 2022 Vorticity-strain rate dynamics and the smallest scales of turbulence. *Phys. Rev. Lett.* **128** (9), 094501.
- BURGERS, J.M. 1948 A mathematical model illustrating the theory of turbulence. *Adv. Appl. Mech.* **1**, 171–199.
- CARBONE, M. & BRAGG, A.D. 2020 Is vortex stretching the main cause of the turbulent energy cascade? *J. Fluid Mech.* **883**, R2.
- CARBONE, M. & WILCZEK, M. 2022 Only two Betchov homogeneity constraints exist for isotropic turbulence. *J. Fluid Mech.* **948**, R2.
- CARDESA, J.I., VELA-MARTÍN, A. & JIMÉNEZ, J. 2017 The turbulent cascade in five dimensions. *Science* **357** (6353), 782–784.
- CHONG, M.S., PERRY, A.E. & CANTWELL, B.J. 1990 A general classification of three-dimensional flow fields. *Phys. Fluids A-Fluid* **2**, 765–777.
- DANISH, M. & MENEVEAU, C. 2018 Multiscale analysis of the invariants of the velocity gradient tensor in isotropic turbulence. *Phys. Rev. Fluids* **3** (4), 044604.
- ELSINGA, G.E., ISHIHARA, T., GOUDAR, M.V., DA SILVA, C.B. & HUNT, J.C.R. 2017 The scaling of straining motions in homogeneous isotropic turbulence. *J. Fluid Mech.* **829**, 31–64.
- ELSINGA, G.E. & MARUSIC, I. 2010 Evolution and lifetimes of flow topology in a turbulent boundary layer. *Phys. Fluids* **22** (1), 015102.
- EYINK, G.L. 2005 Locality of turbulent cascades. *Phys. D: Nonlinear Phenom.* **207** (1-2), 91–116.
- HAMLINGTON, P.E., SCHUMACHER, J. & DAHM, W.J.A. 2008 Local and nonlocal strain rate fields and vorticity alignment in turbulent flows. *Phys. Rev. E* **77** (2), 026303.
- JIMÉNEZ, J., WRAY, A.A., SAFFMAN, P.G. & ROGALLO, R. 1993 The structure of intense vorticity in isotropic turbulence. *J. Fluid Mech.* **255**, 65–90.
- JOHNSON, P.L. 2020 Energy transfer from large to small scales in turbulence by multiscale nonlinear strain and vorticity interactions. *Phys. Rev. Lett.* **124** (10), 104501.
- KANEDA, Y. & ISHIHARA, T. 2006 High-resolution direct numerical simulation of turbulence. *J. Turbul.* **7**, N20.
- LEUNG, T., SWAMINATHAN, N. & DAVIDSON, P.A. 2012 Geometry and interaction of structures in homogeneous isotropic turbulence. *J. Fluid Mech.* **710**, 453–481.

- LOZANO-DURÁN, A., HOLZNER, M. & JIMÉNEZ, J. 2016 Multiscale analysis of the topological invariants in the logarithmic region of turbulent channels at a friction Reynolds number of 932. *J. Fluid Mech.* **803**, 356–394.
- MENEVEAU, C. 2011 Lagrangian dynamics and models of the velocity gradient tensor in turbulent flows. *Annu. Rev. Fluid Mech.* **43**, 219–245.
- OHKITANI, K. 1994 Kinematics of vorticity: vorticity-strain conjugation in incompressible fluid flows. *Phys. Rev. E* **50** (6), 5107.
- OHKITANI, K. & KISHIBA, S. 1995 Nonlocal nature of vortex stretching in an inviscid fluid. *Phys. Fluids* **7** (2), 411–421.
- PUMIR, A. 1994 A numerical study of pressure fluctuations in three-dimensional, incompressible, homogeneous, isotropic turbulence. *Phys. Fluids* **6** (6), 2071–2083.
- TSINOBER, A. 2000 Vortex stretching versus production of strain/dissipation. In *Turbulence Structure and Vortex Dynamics*, vol. 164, p. 191. Cambridge University Press.
- TSINOBER, A. 2001 *An Informal Introduction to Turbulence*, vol. 63. Springer Science & Business Media.
- TSUJI, Y. & ISHIHARA, T. 2003 Similarity scaling of pressure fluctuation in turbulence. *Phys. Rev. E* **68** (2), 026309.
- VLAYKOV, D.G. & WILCZEK, M. 2019 On the small-scale structure of turbulence and its impact on the pressure field. *J. Fluid Mech.* **861**, 422–446.
- WILCZEK, M. & MENEVEAU, C. 2014 Pressure Hessian and viscous contributions to velocity gradient statistics based on Gaussian random fields. *J. Fluid Mech.* **756**, 191–225.
- YANG, P.-F., ZHOU, Z.D., XU, H. & HE, G.W. 2023 Strain self-amplification is larger than vortex stretching due to an invariant relation of filtered velocity gradients. *J. Fluid Mech.* **955**, A15.